Split singularities and dislocation injection in strained silicon

Martijn Feron, Zhen Zhang,[a] and Zhigang Suo[b]
School of Engineering and Applied Sciences, Harvard University, Cambridge, Massachusetts 02138

Martijn Feron
Faculty of Mechanical Engineering, Technische Universiteit Eindhoven, 5600 MB, The Netherlands

(Received 6 February 2007; accepted 31 May 2007; published online 16 July 2007)

In a microelectronic device, the strain field may be intensified at a sharp feature, such as an edge or a corner, injecting dislocations into silicon and ultimately failing the device. The strain field at an edge is singular and is often a linear superposition of two modes of different exponents. We characterize the relative contribution of the two modes by a mode angle, and determine the critical slip systems as the amplitude of the load increases. We calculate the critical residual stress in a thin-film stripe bonded on a silicon substrate. © *2007 American Institute of Physics*.
[DOI: 10.1063/1.2753674]

I. INTRODUCTION

In microelectronic devices, strains are deliberately introduced into silicon to increase the mobility of electrons or holes; see Ref. 1 for a review. The strains, however, may cause mechanical failure. In particular, the devices usually contain sharp features such as edges and corners, which may intensify strains and inject dislocations into silicon, failing the devices.[2,3] We recently described a method to predict conditions under which such sharp features do not inject dislocations.[4] The method is further developed in the present paper to account for split singularities.[5,6]

Figure 1 illustrates the structure to be studied. A blanket film, of thickness h and residual stress σ, is grown on the (001) surface of a single-crystal silicon substrate. The film is then patterned into a stripe of width L, with the side surfaces parallel to the (110) plane of silicon. When the film covers the entire surface of the substrate, the film is in a state of uniform stress, and the substrate is stress-free. When the film is patterned into a stripe, a field of stress builds up in the substrate and concentrates at the root of each edge. It is this concentrated stress that injects dislocations into silicon.

The structure in Fig. 1 is similar to those studied in Refs. 4 and 7–12, but this paper will examine a specific aspect: split singularities. It is well known that, at the tip of a crack in a homogeneous elastic material, under the plane strain conditions, the singular stress field is a linear superposition of two modes, the tensile mode and the shearing mode, both modes having the exponent of $\frac{1}{2}$. More generally, at the tip of bonded wedges of dissimilar materials, the singular stress field may still consist of two modes, but usually of *unequal exponents*, either a pair of complex conjugates or two unequal real numbers.[6,13–16] The case of complex-conjugate exponents has been extensively discussed within the context of a crack lying on a bimaterial interface.[17] The present paper will focus on the case that the two modes have unequal real exponents, that is, a stronger and a weaker singularity coexist. It has been shown that both singularities can be important in causing failure.[5,6,16] Section II will describe the linear superposition of two modes of singular stress fields. Section III will investigate which slip systems will firstly be activated. Section IV will calculate the critical residual stress in the thin-film stripe for injecting dislocations into the silicon substrate.

II. A LINEAR SUPERPOSITION OF TWO MODES OF SINGULAR STRESS FIELDS

The inset of Fig. 2 illustrates an edge of the thin film bonded on the substrate, along with a system of polar coordinates (r,θ,z). In the view of the root of the edge, the film takes the quarter space, $0° \leqslant \theta \leqslant 90°$, and the substrate takes the half space, $-180° \leqslant \theta \leqslant 0°$. The two materials are bonded along the interface, $\theta = 0°$. Both materials are taken to be

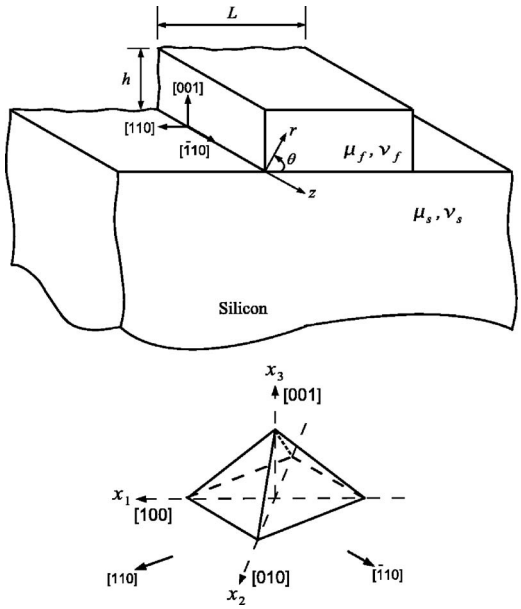

FIG. 1. A blanket thin film, of thickness h and residual stress σ, is grown on the (001) surface of a single-crystal silicon substrate. The film is then patterned into a stripe of width L, with the side surfaces parallel to the (110) plane of silicon.

[a]Electronic mail: zhen.zhang@post.harvard.edu
[b]Electronic mail: suo@deas.harvard.edu

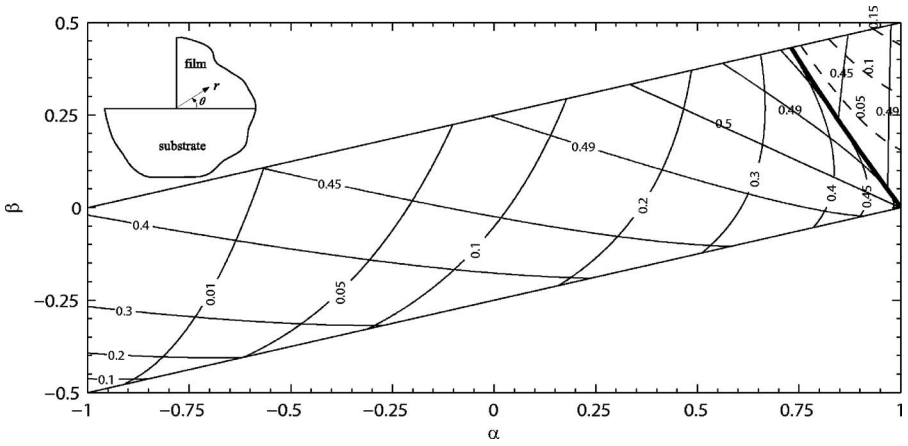

FIG. 2. The inset shows the root of an edge of a thin film bonded on a substrate. Contours of the singular exponents are plotted on the plane of the Dundurs parameters (α,β). The parallelogram is divided into two regions by a dark curve. In the lower-left region, the exponents are two unequal real numbers, with the larger one labeled horizontally and the smaller one labeled vertically. In the upper-right region, the exponents are a pair of complex conjugates, with the real part depicted by solid lines and labeled horizontally and the imaginary part depicted by dashed lines and labeled vertically.

elastic and isotropic. For problems of this type Dundurs[18] showed that the stress field depends on elastic constants through two dimensionless parameters:

$$\alpha = \frac{\mu_f(1-\nu_s) - \mu_s(1-\nu_f)}{\mu_f(1-\nu_s) + \mu_s(1-\nu_f)}, \tag{1}$$

$$\beta = \frac{1}{2}\left[\frac{\mu_f(1-2\nu_s) - \mu_s(1-2\nu_f)}{\mu_f(1-\nu_s) + \mu_s(1-\nu_f)}\right], \tag{2}$$

where μ is the shear modulus and ν is Poisson's ratio. The subscripts f and s refer to the film and the silicon substrate, respectively. By requiring $0 \leqslant \nu \leqslant 0.5$ and $\mu > 0$, the Dundurs parameters are confined within a parallelogram in the (α,β) plane, with vertices at (1,0), (1,0.5), (−1,0), and (−1,−0.5).

For a singular field around the root of the edge, each component of the stress tensor, say $\sigma_{\theta\theta}$, takes the form of $\sigma_{\theta\theta} \sim r^{-\lambda}$. This singular stress field is determined by an eigenvalue problem, resulting in a transcendental equation that determines the exponent λ.[19–21] The exponent is restricted as $0 < \mathrm{Re}(\lambda) < 1$, a restriction commonly adopted, with justifications criticized in Refs. 22 and 23. For the specific geometry illustrated in the inset, Fig. 2 plots the contours of the exponents on the (α,β) plane. The parallelogram is divided into two regions by a dark curve. In the lower-left region, the exponents are two unequal real numbers, one stronger (λ_1) and the other weaker (λ_2). The values for λ_1 are labeled horizontally, and those for λ_2 are labeled vertically. In the whole region, $\lambda_2 < \lambda_1 \leqslant 0.5$. In the upper-right region, the exponents are a pair of complex conjugates, $\lambda_{1,2} = \xi \pm i\varepsilon$. The real part is depicted by solid lines and labeled horizontally, while the imaginary part is depicted by dashed lines and labeled vertically. At each point on the boundary (i.e., the dark curve), the two exponents degenerate to one value: when the point is approached from a region of real exponents, the two real exponents become identical; when the point is approached from a region of complex-conjugate exponents, the imaginary part vanishes. When $\alpha = 1$, i.e., the film is rigid, the singularity exponents are the same as those for an interfacial crack, $\lambda_{1,2} = 0.5 \pm i\varepsilon$, with $\varepsilon = 1/(2\pi)\ln[(1-\beta)/(1+\beta)]$.[24]

As noted in Ref. 5, when the two materials have similar elastic constants, i.e., when $\alpha = \beta = 0$, the two modes of singular fields can be interpreted readily. In this case, the line bisecting the angle of the wedge is a line of symmetry. The stronger mode corresponds to a stress field symmetric about this line (i.e., the tensile mode). The weaker mode corresponds to a stress field antisymmetric about this line (i.e., the shearing mode). When the two materials have dissimilar elastic constants, however, the symmetry is broken, and the two modes may not be interpreted in such a simple way.

Following a common practice, in this paper we will use α to represent the elastic mismatch and neglect the effect of β by setting $\beta = 0$. When $\beta = 0$, the exponents are two unequal real numbers, regardless of the values of α.

We next paraphrase several fundamental ideas in fracture mechanics.[25] Once we retain the two unequal exponents, the stress field around the root of the edge is a linear superposition of the two modes:

$$\sigma_{ij}(r,\theta) = \frac{k_1}{(2\pi r)^{\lambda_1}}\Sigma_{ij}^1(\theta) + \frac{k_2}{(2\pi r)^{\lambda_2}}\Sigma_{ij}^2(\theta). \tag{3}$$

The angular functions $\Sigma_{ij}^1(\theta)$ and $\Sigma_{ij}^2(\theta)$ are normalized such that $\Sigma_{r\theta}^1(0) = \Sigma_{r\theta}^2(0) = 1$, and their full expressions are listed in the Appendix. The stress intensity factors, k_1 and k_2, are determined by the external boundary conditions, as described in Sec. IV.

The singular stress field [Eq. (3)] is obtained by assuming that the materials are elastic, and the edge is perfectly sharp. Such assumptions are invalid in a process zone around the root of the edge. Let Λ be the size of the process zone, within which the singular stress field [Eq. (3)] is invalid. Also, the singular stress field [Eq. (3)] is invalid at length scale h, where the external boundary conditions will change the stress distribution. However, provided the process zone is significantly smaller than the macroscopic length, $\Lambda \ll h$, the singular stress field [Eq. (3)] prevails within an annulus, known as the k annulus, of some radii bounded between Λ and h.

The two parameters, k_1 and k_2, have different dimensions, (stress)(length)$^{\lambda_1}$ and (stress)(length)$^{\lambda_2}$, respectively. We introduce a convention by writing

$$k_1 = S\Lambda^{\lambda_1}\cos\psi, \quad k_2 = S\Lambda^{\lambda_2}\sin\psi. \tag{4}$$

This convention is illustrated in Fig. 3. Here S and ψ characterize the stress field at length scale Λ, with S characterizing the amplitude of the stress field and ψ characterizing the

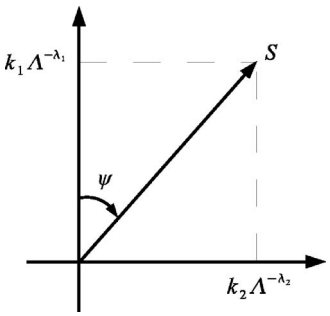

FIG. 3. The graphical representation of the amplitude S and the mode angle ψ.

relative contribution of the two modes. Since both k_1 and k_2 can be either positive or negative, the mode angle can be in the entire range of $0 \leqslant \psi < 360°$.

The microscopic process of dislocation injection occurs within the process zone but is driven by the stress field [Eq. (3)] in the k annulus. Dislocations inject from the root when the amplitude S reaches a critical value S_c, namely,

$$S(\psi) = S_c(\psi). \tag{5}$$

The amplitude S and the mode angle ψ are determined by the external boundary conditions, by solving a boundary value problem of linear elasticity. The critical condition $S_c(\psi)$ is determined either by experimental measurement or by computation from a microscopic model of the injecting process.[4]

III. SELECTION OF CRITICAL SLIP SYSTEM

Table I lists the 12 slip systems in silicon. Given a mode angle ψ as the amplitude S increases, some slip systems will activate earlier than others. We select the critical slip systems by the following procedure. For each slip system, we use the stress field [Eq. (3)] to calculate the resolved shear stress at distance $r=\Lambda$. The slip system with the maximum resolved shear stress is taken to be the critical slip system, on which dislocations are firstly injected. Observe that the dislocation injection is a thermally activated atomic process and that actual dislocation injection occurs more likely during device processing at higher temperature and cross-slip can also occur. Such consideration is beyond the scope of this paper.

TABLE I. The 12 slip systems and the corresponding critical polar angles.

Slip plane n	Slip direction b	Critical polar angle θ^*
(111)	$[\bar{1}10]$	−125.26°
	$[10\bar{1}]$	−125.26°
	$[01\bar{1}]$	−125.26°
$(1\bar{1}1)$	[110]	Fig. 4[a]
	$[10\bar{1}]$	−125.26°
	$[0\bar{1}\bar{1}]$	−54.74°
$(\bar{1}\bar{1}1)$	$[\bar{1}10]$	−54.74°
	$[0\bar{1}\bar{1}]$	−54.74°
	$[\bar{1}0\bar{1}]$	−54.74°
$(\bar{1}11)$	[110]	Fig. 4[a]
	$[\bar{1}0\bar{1}]$	−54.74°
	$[01\bar{1}]$	−125.26°

[a]For slip systems $\frac{1}{2}(1\bar{1}1)[110]$ and $\frac{1}{2}(\bar{1}11)[110]$, the critical polar angle, i.e., the polar angle for which the resolved shear stress has a maximum, depends on the mode angle. This dependence is depicted in Fig. 4.

For a given slip system, let n_i be the unit vector normal to the slip plane and b_j be the Burgers vector. Under a general state of stress σ_{ij}, the resolved shear stress on the slip system is

$$\tau_{nb} = |\sigma_{ij} n_i b_j|/b. \tag{6}$$

A combination of Eqs. (3), (4), and (6) gives the resolved shear stress at the distance $r=\Lambda$ by

$$\frac{\tau_{nb}}{S} = \left| \cos\psi \frac{\Sigma_{ij}^1(\theta) n_i b_j}{(2\pi)^{\lambda_1} b} + \sin\psi \frac{\Sigma_{ij}^2(\theta) n_i b_j}{(2\pi)^{\lambda_2} b} \right|. \tag{7}$$

Because this procedure invokes only the magnitude of the resolved shear stress and not the direction, a simultaneous change in the sign of the stress intensity factors k_1 and k_2 will not change the condition of dislocation injection. Consequently, we can restrict the range of the mode angle to $-90° \leqslant \psi \leqslant 90°$. Indeed, the right-hand side of Eq. (7) is a function of ψ with a period of 180°.

An inspection of Fig. 1 shows that the slip systems $\frac{1}{2}(111)[\bar{1}10]$ and $\frac{1}{2}(\bar{1}\bar{1}1)[\bar{1}10]$ are of zero resolved shear stress. The slip systems $\frac{1}{2}(111)[10\bar{1}]$ and $\frac{1}{2}(111)[01\bar{1}]$ are of identical resolved shear stress and with fixed polar angle $\theta = -125.26°$. Other similar pairs of slip systems are listed in Table I. By contrast, the resolved shear stress for slip systems $\frac{1}{2}(1\bar{1}1)[110]$ and $\frac{1}{2}(\bar{1}11)[110]$ is a function of polar angle θ. As an example, in Fig. 4(a), the resolved shear stress is plotted as a function of θ for $\psi=0$ and $\alpha=0.5$. The polar angle θ^* corresponding to the maximum resolved shear stress is selected as the critical angle where the dislocation is injected. In Fig. 4(b), the critical polar angle θ^* in the loading range $-90° \leqslant \psi \leqslant 90°$ is plotted for $\alpha=0.5$. This procedure can be repeated for all values of α.

For $\alpha=0.5$, Fig. 5(a) plots the resolved shear stresses as a function of the mode angle ψ for all 12 slip systems. The slip system with the largest resolved shear stress is the critical slip system on which dislocations are firstly injected. The slip systems selected in such a way are marked as the critical slip system for the whole range value of $-90° \leqslant \psi \leqslant 90°$. Obviously, different slip systems can be activated for different values of mode angle ψ. Similarly, the critical slip systems for any material combination under any mode angle can be selected, such as shown in Fig. 5(b) for $\alpha=0$ and in Fig. 5(c) for $\alpha=-0.5$.

IV. THE CRITICAL CONDITION FOR DISLOCATION INJECTION

The stress field around the root of the edge is described by Eq. (3). Linearity and dimensional consideration dictate that the stress intensity factors k_1 and k_2 should take the form

$$k_1 = \sigma h^{\lambda_1} f_1(L/h, \alpha), \quad k_2 = \sigma h^{\lambda_2} f_2(L/h, \alpha), \tag{8}$$

where the dimensionless functions $f_1(L/h, \alpha)$ and $f_2(L/h, \alpha)$ are determined as follows. We calculate the full stress field in

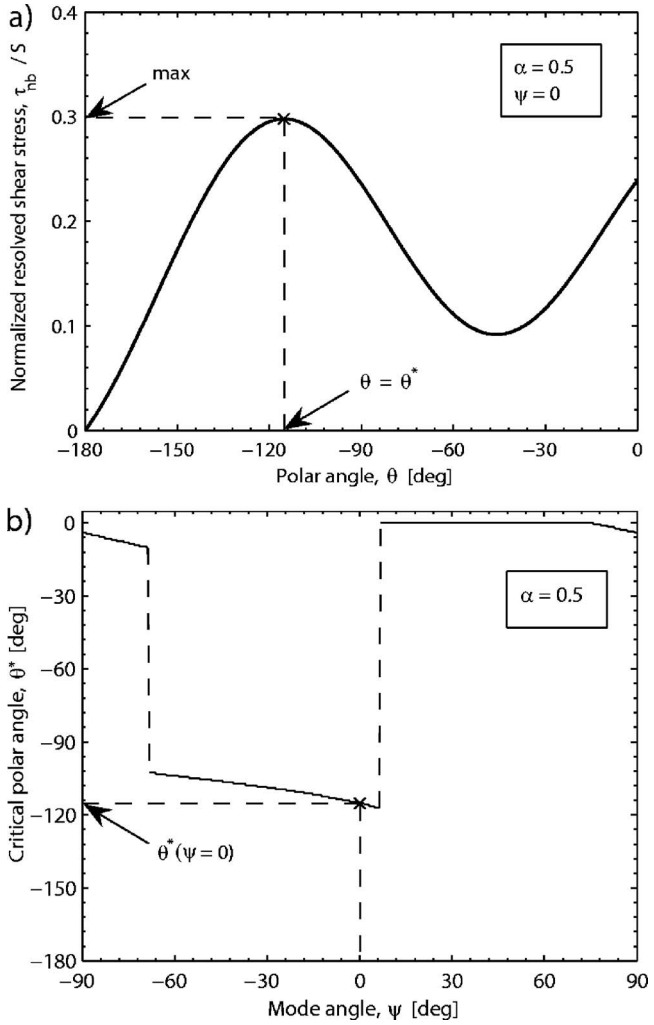

FIG. 4. The normalized resolved shear stress for slip systems $\frac{1}{2}(1\bar{1}1)[110]$ and $\frac{1}{2}(\bar{1}11)[110]$ is a function of the polar angle θ. As an example, in (a), the normalized shear stress is plotted as a function of θ. The polar angle θ^* corresponding to the maximum resolved shear stress is selected and marked by "×" as the critical angle where the potential dislocation is nucleated. In (b), all the critical polar angles θ^* in the range $-90° \leqslant \psi \leqslant 90°$ are plotted for α=0.5.

the structure by using the finite element package ABAQUS6.6 then fit the interfacial shear stress close to the root, say, $10^{-3} < r/h < 10^{-2}$, to the equation

$$\sigma_{r\theta}(\theta = 0) = \frac{k_1}{(2\pi r)^{\lambda_1}} + \frac{k_2}{(2\pi r)^{\lambda_2}}, \tag{9}$$

with k_1 and k_2 as fitting parameters. The two functions so calculated are plotted in Fig. 6. The trend is understood as follows. Although the stress field intensifies at the root, the side surface of the stripe is traction-free. When the stripe is very narrow, $L/h \to 0$, the stress in the stripe is almost fully relaxed, so f_1 and f_2 go to zero. When the stripe is very wide, $L/h \to \infty$, the stress field near one edge of the stripe no longer feels the presence of the other edge, so f_1 and f_2 attain plateaus.

A combination of Eqs. (4) and (8) gives the mode angle ψ as[6]

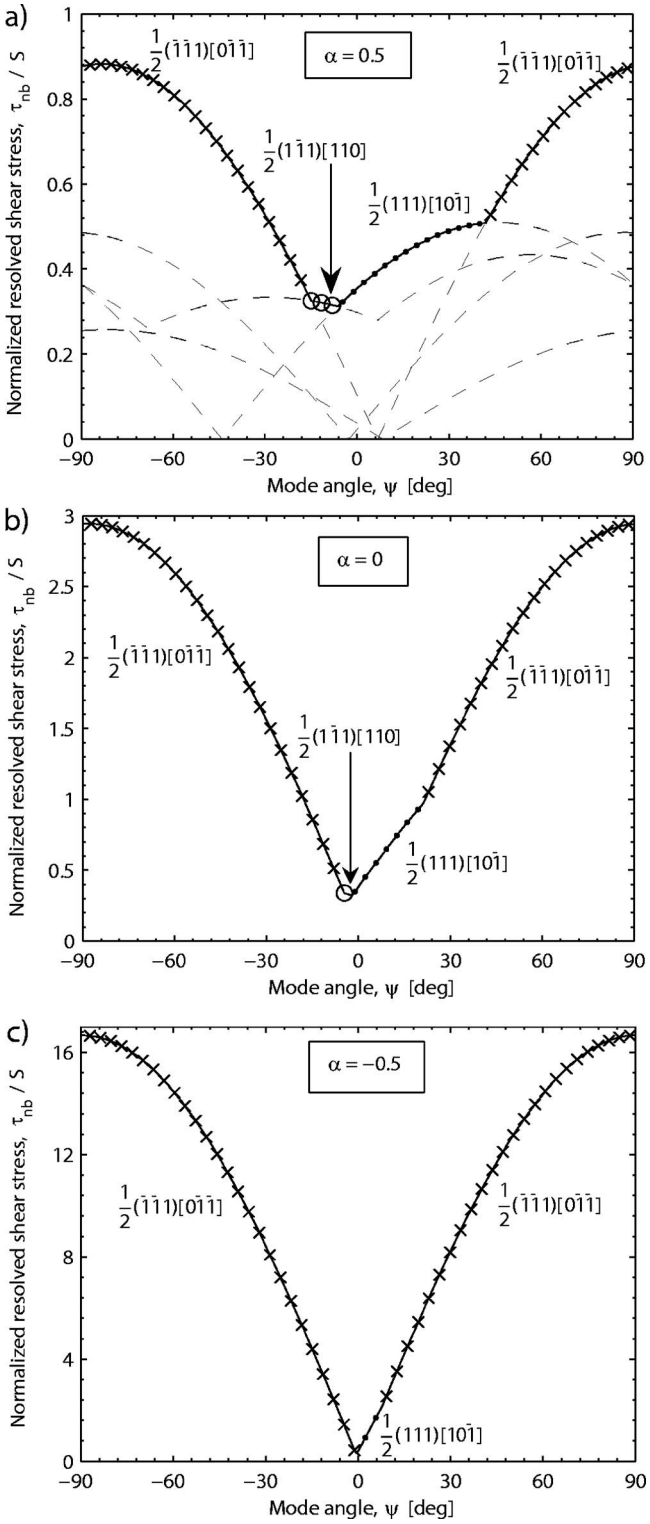

FIG. 5. Normalized resolved shear stresses are plotted as a function of mode angle for all of the 12 slip systems. The slip system with the largest resolved shear stress is the potential slip system on which the dislocation is firstly injected, so those slip systems are selected and marked for the whole range of the mode angle, $-90° \leqslant \psi \leqslant 90°$: (a) α=0.5, (b) α=0, and (c) α=−0.5.

$$\tan\psi = \frac{f_2}{f_1}\left(\frac{\Lambda}{h}\right)^{\lambda_1 - \lambda_2}. \tag{10}$$

Take the typical value of film thickness h=100 mn and take the process zone size Λ to be the Burgers vector of silicon,

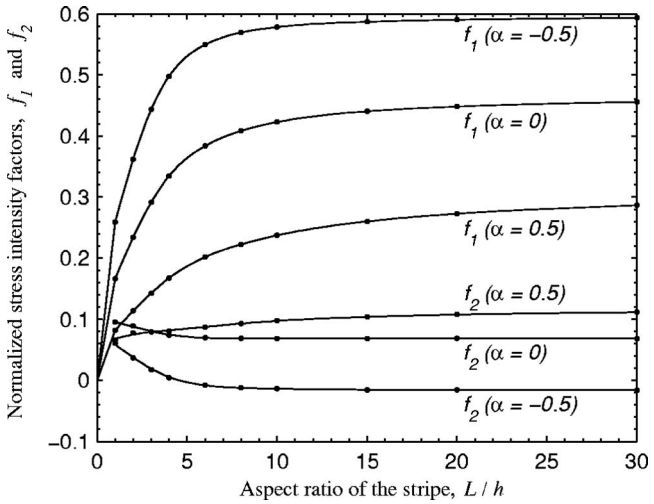

FIG. 6. The normalized stress intensity factors, f_1 and f_2, are plotted as a function of the aspect ratio, L/h, of the stripe on the silicon substrate.

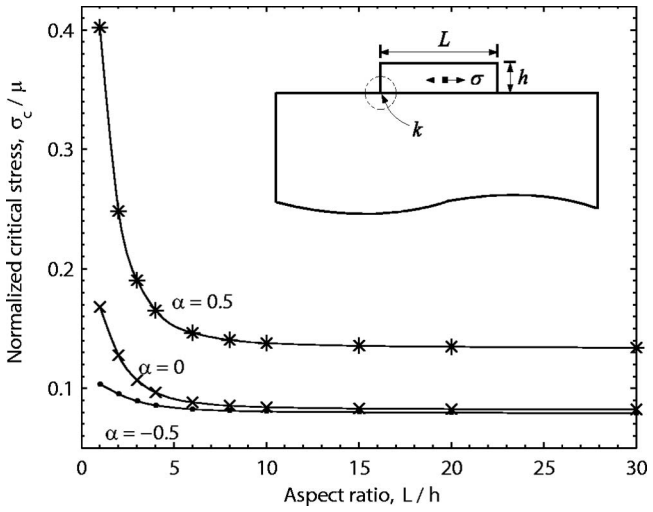

FIG. 8. Normalized critical stresses are plotted as a function of the aspect ratio L/h for Dundurs parameter $\alpha=0.5,0,-0.5$.

$b=0.383$ mn. Figure 7 plots the mode angle ψ as a function of the Dundurs parameter α for the aspect ratio of the stripe, $L/h=2$ and 20. We observe that for the values of $\alpha<0$, i.e., when the film is more compliant than the substrate, both the elastic mismatch and the aspect ratio have negligible effects on the mode angle ψ, and the weaker singular term in Eq. (3) is negligible, so that the singular stress field can be simplified to the single mode. However, for positive values of α, i.e., when the film is stiffer than the substrate, the mode angle ψ increases very fast, and both singular terms in Eq. (3) should be taken into account.

We now comment on the case studied in Ref. 4. The film stripe is SiN with shear modulus of 54.3 GPa and Poisson's ratio of 0.27. The silicon substrate is of shear modulus of 68.1 GPa and Poisson's ratio of 0.22. The elastic mismatch is small, $\alpha\approx 0$. The singularity exponents are $\lambda_1=0.4514$ and $\lambda_2=0.0752$. Still taking $h=100$ mn and $b=0.383$ mn, we obtain that $\psi=0.2°$ for $L/h=20$ and $\psi=1.27°$ for $L/h=2$. Evidently in this case the weaker singularity makes negligible contribution. From Fig. 5(b), we identify that the critical slip systems are $\frac{1}{2}(111)[01\bar{1}]$ and $\frac{1}{2}(111)[10\bar{1}]$. In the experiment by Isomae,[10] i.e., Fig. 14 in Ref. 10, two groups of dislocations were observed along the edge, one on slip system $\frac{1}{2}(111)[01\bar{1}]$ and the other on $\frac{1}{2}(111)[10\bar{1}]$. This is consistent with the analysis in the present paper and was also predicted in Ref. 4.

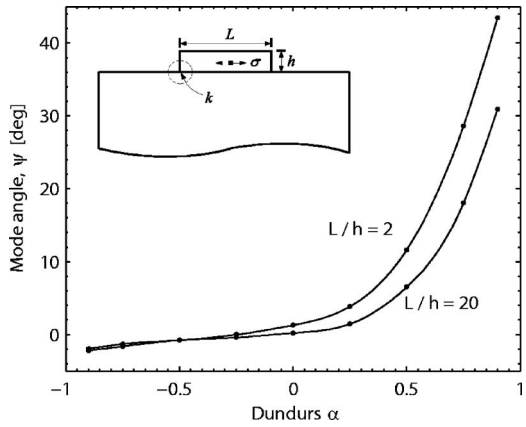

FIG. 7. Mode angle ψ is plotted as a function of Dundurs parameter α for the aspect ratio of the stripe, $L/h=2$ and 20.

We now calculate the critical residual stress in the thin-film stripe to inject dislocations into silicon. We assume that the critical condition is reached when the maximum resolved shear stress reaches the theoretical shear strength at distance $r=b$. The theoretical shear strength is estimated by $\tau_{\text{th}}=0.2\mu$, where μ is the shear modulus of silicon.[26] Setting $\tau_{nb}(b)=\tau_{\text{th}}$, a combination of Eqs. (3), (6), and (8) gives a scaling relation between the critical residual stress and the feature sizes:

$$\frac{\sigma_c}{\mu}=0.2\left\{\left|\left[\left(\frac{h}{b}\right)^{\lambda_1}\frac{\Sigma_{ij}^1(\theta)}{(2\pi)^{\lambda_1}}f_1+\left(\frac{h}{b}\right)^{\lambda_2}\frac{\Sigma_{ij}^2(\theta)}{(2\pi)^{\lambda_2}}f_2\right]\frac{n_i b_j}{b}\right|\right\}^{-1}. \tag{11}$$

In Fig. 8, we plot the normalized critical stresses as a function of the aspect ratio L/h for Dundurs $\alpha=0.5,0,-0.5$. A plateau is reached for large values of the aspect ratio L/h. When the aspect ratio is decreased, the critical stress will drastically improve, implying the fact that a narrow stripe might not inject dislocations into the silicon substrate, while a wide stripe could inject dislocations. Also evident is that the critical stress increases as the film becomes stiffer. This is because the same level of residual stress in a stiff film will induce a lower level of stress in the silicon substrate.

V. CONCLUDING REMARKS

The singular stress field at the root of an edge is a linear superposition of two modes with different exponents. A mode angle ψ is introduced to measure the relative contribution of the two modes to the failure conditions. Figure 2 shows that the two exponents are very different when the film is compliant relative to silicon and are very similar when the film is stiff relative to silicon. Consequently, as shown in Fig. 7, the weaker singular term in Eq. (3) is negligible when the film is compliant but is significant when the film is stiff. For the full range of the mode angle, we describe

TABLE II. Singularity exponents and the associated coefficients in Eqs. (A1)–(A5) in silicon substrate for $\alpha = 0.5, 0, -0.5$ with $\beta = 0$.

α	−0.5		0		0.5	
λ	0.4314	0.0168	0.4555	0.0915	0.4783	0.2542
A	0.9803	−0.3775	0.9885	0.1427	0.9951	0.4213
B	0.2687	−9.6738	0.3695	−1.9826	0.4717	−0.9088
C	−0.5123	−105.1100	−0.6804	−9.0562	−0.8414	−2.3815
D	1.8693	4.1015	1.8201	−0.6517	1.7750	−1.1040

a procedure to select the critical slip systems. On the basis of the criterion that dislocations inject when the resolved shear stress at distance b from the root of the edge reaches the theoretical strength, we calculate the critical residual stress in the stripe and show that the critical stress is low when the stripe is wide or compliant.

ACKNOWLEDGMENTS

This work is carried out when the authors are supported by Intel Corporation through a contract via the Semiconductor Research Corporation (Award No. 2005-KJ-1369) and by the National Science Foundation through the MRSEC at Harvard University.

APPENDIX: STRESS COMPONENTS IN POLAR COORDINATES AND CRYSTAL COORDINATES

The singular stress field [Eq. (3)] is solved by the methods outlined in Refs. 5 and 20. The eigenfunctions $\Sigma_{ij}(\theta)$ associated with the eigenvalue λ are expressed in polar coordinates (r, θ, z) as

$$\Sigma_{rr}(\theta) = -(\lambda-1)\{(\lambda-2)[A\sin(\lambda-2)\theta + B\cos(\lambda-2)\theta] + (\lambda+2)[C\sin\lambda\theta + D\cos\lambda\theta]\}, \tag{A1}$$

$$\Sigma_{\theta\theta}(\theta) = (\lambda-1)(\lambda-2)[A\sin(\lambda-2)\theta + B\cos(\lambda-2)\theta + C\sin\lambda\theta + D\cos\lambda\theta], \tag{A2}$$

$$\Sigma_{r\theta}(\theta) = (\lambda-1)\{(\lambda-2)[A\cos(\lambda-2)\theta - B\sin(\lambda-2)\theta] + \lambda(C\cos\lambda\theta - D\sin\lambda\theta)\}, \tag{A3}$$

$$\Sigma_{zz}(\theta) = -4\nu(\lambda-1)(C\sin\lambda\theta + D\cos\lambda\theta), \tag{A4}$$

$$\Sigma_{rz} = \Sigma_{\theta z} = 0. \tag{A5}$$

The eigenvalue λ and its associated coefficients A, B, C, and D in the film and the substrate are solved by the boundary conditions. In this paper, the singular stress field in the silicon substrate around the root of the edge causes dislocation to be injected, so that the eigenvalues and the associated coefficients only in the substrate are listed in Table II (for $\alpha = 0.5, 0, -0.5$ with $\beta = 0$).

In calculating the resolved shear stress [Eq. (6)], the stress components in the crystal coordinates (x_1, x_2, x_3), σ_{ij}, are converted from those in the polar coordinates (r, θ, z). The relation of (x_1, x_2, x_3) and (r, θ, z) is depicted in Fig. 1, and the matrix of conversion is

$$[Q] = \begin{bmatrix} -\cos\theta/\sqrt{2} & -\cos\theta/\sqrt{2} & \sin\theta \\ \sin\theta/\sqrt{2} & \sin\theta/\sqrt{2} & \cos\theta \\ -1/\sqrt{2} & 1/\sqrt{2} & 0 \end{bmatrix}. \tag{A6}$$

From $[\sigma]_{\text{crystal}} = [Q]^T[\sigma]_{\text{polar}}[Q]$, the stress components in the crystal coordinates are

$$\sigma_{11} = \sigma_{22} = (\sigma_{rr}\cos^2\theta + \sigma_{\theta\theta}\sin^2\theta + \sigma_{zz} - \sigma_{r\theta}\sin 2\theta)/2, \tag{A7}$$

$$\sigma_{12} = \sigma_{21} = (\sigma_{rr}\cos^2\theta + \sigma_{\theta\theta}\sin^2\theta - \sigma_{zz} - \sigma_{r\theta}\sin 2\theta)/2, \tag{A8}$$

$$\sigma_{13} = \sigma_{31} = \sigma_{23} = \sigma_{32} = [(\sigma_{\theta\theta} - \sigma_{rr})\sin 2\theta - 2\sigma_{r\theta}\cos 2\theta]/2\sqrt{2}, \tag{A9}$$

$$\sigma_{33} = \sigma_{rr}\sin^2\theta + \sigma_{\theta\theta}\cos^2\theta + \sigma_{r\theta}\sin 2\theta. \tag{A10}$$

[1] M. Ieong, B. Doris, J. Kedzierski, K. Rim, and M. Yang, Science **306**, 2057 (2004).
[2] M. Dellith, G. R. Booker, B. O. Kolbesen, W. Bergholz, and F. Gelsdorf, J. Electrochem. Soc. **143**, 210 (1996).
[3] M. Miyake and M. Takahashi, J. Electrochem. Soc. **144**, 1020 (1997).
[4] Z. Zhang, J. Yoon, and Zhigang Suo, Appl. Phys. Lett. **89**, 261912 (2006).
[5] X. H. Liu, Z. Suo, and Q. Ma, Acta Mater. **47**, 67 (1999).
[6] Z. Zhang and Z. Suo, Int. J. Solids Struct. **44**, 4559 (2007).
[7] M. Kammler, D. Chidambarrao, K. W. Schwarz, C. T. Black, and F. M. Ross, Appl. Phys. Lett. **87**, 133116 (2005).
[8] S. M. Hu, Appl. Phys. Lett. **32**, 5 (1978); J. Appl. Phys. **50**, 4661 (1979); **70**, R53 (1991).
[9] S. C. Jain, H. E. Maes, K. Pinardi, and I. De Wolf, J. Appl. Phys. **79**, 8145 (1996).
[10] S. Isomae, J. Appl. Phys. **52**, 2782 (1981).
[11] J. Vanhellemont, S. Amelinckx, and C. Claeys, J. Appl. Phys. **61**, 2170 (1987); **61**, 2176 (1987); **63**, 5703 (1988).
[12] K. W. Schwarz and D. Chidambarrao, J. Appl. Phys. **85**, 7198 (1999).
[13] A. R. Akisanya and N. A. Fleck, Int. J. Solids Struct. **34**, 1645 (1997).
[14] I. Mohammed and K. M. Liechti, J. Mech. Phys. Solids **48**, 735 (2000).
[15] E. D. Reedy, Int. J. Solids Struct. **37**, 2429 (2000).
[16] P. E. W. Labossiere, M. L. Dunn, and S. J. Cunningham, J. Mech. Phys. Solids **50**, 405 (2002).
[17] J. R. Rice, J. Appl. Mech. **55**, 98 (1988).
[18] J. Dundurs, J. Appl. Mech. **36**, 650 (1969).
[19] M. L. Williams, J. Appl. Mech. **19**, 526 (1952).
[20] D. B. Bogy, J. Appl. Mech. **38**, 377 (1971).
[21] J. R. Barber, *Elasticity*, 2nd ed. (Kluwer, Dordrecht, 2002).
[22] C. Y. Hui and A. Ruina, Int. J. Fract. **72**, 97 (1995).
[23] M. L. Dunn, C. Y. Hui, P. E. W. Labossiere, and Y. Y. Lin, Int. J. Fract. **110**, 101 (2001).
[24] N. Lu, J. Yoon, and Z. Suo, Int. J. Mat. Res. **98**(7), special issue for Wolfgang Pompe 65th birthday (2007).
[25] B. Lawn, *Fracture of Brittle Solids*, 2nd ed. (Cambridge University Press, Cambridge, 1993).
[26] J. P. Hirth and J. Lothe, *Theory of Dislocation*, 2nd ed. (Krieger, Malabar, FL, 1992), p. 6.